The Empty Ring Rule: A Universal Aromaticity Code for Engineering Magnetic Nanographenes

Aristides D. Zdetsis*

Molecular Engineering Laboratory, Department of Physics, University of Patras, Patras 26500 GR, Greece.

Supporting Information

§S1. The general Picture

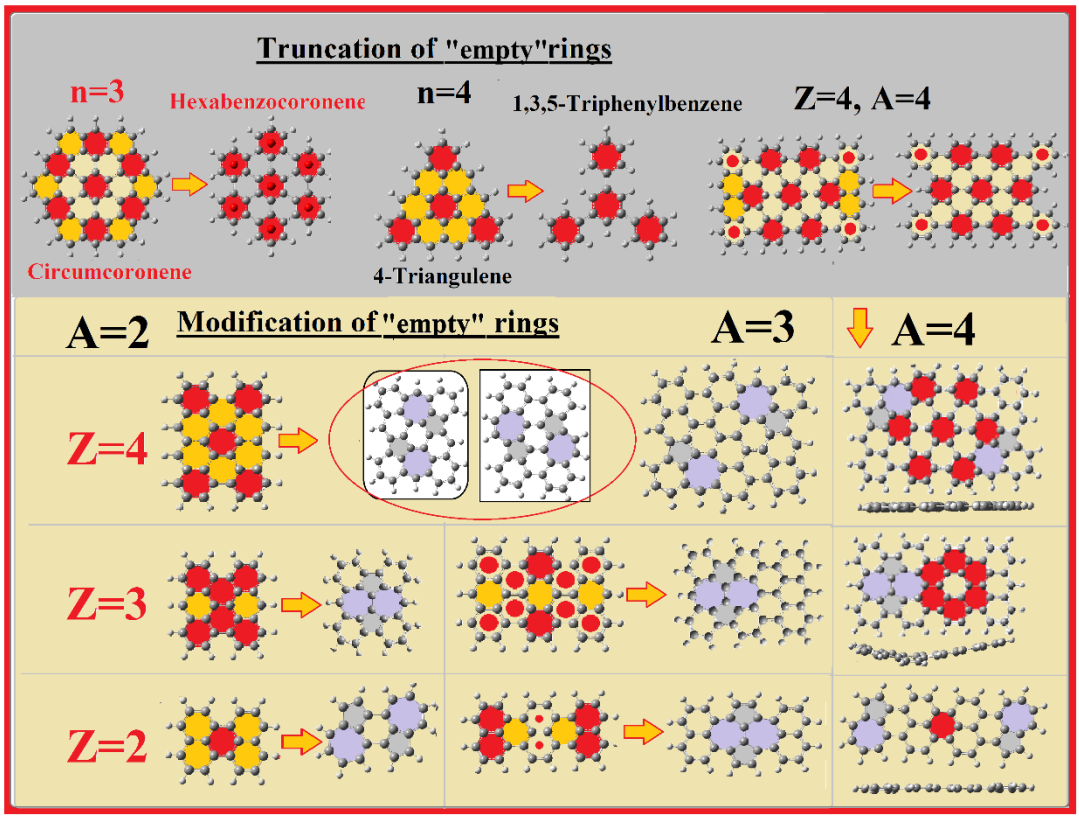

An Extended Graphical Summary. *In analogy to the functional truncation of "empty" (yellow online) rings in circum-coronene and other nanographenes (top), ERR not only accounts for the behavior of recently synthesized SW-AGNRs but also predicts a lower-energy 4×2 SW isomer with an identical excitation spectrum yet a clearly differentiated Raman response. Moreover, ERR reveals that Z=4 AGNRs and their*

SW-modified analogues possessing Clar-type aromaticity patterns are inherently more stable, aromatic, and planar than Z=3 or Z=2 systems, the latter showing strong odd–even variations in their magnetic, electronic, and structural properties. All calculation Presented in this work were performed using the Gaussian 16 software package.[S1]

§S1.2. Aromaticity Patterns and "partially empty" rings

The aromaticity patterns (APs) are **structural fingerprints** of π-electron distribution, and as such they are expected to correlate strongly with **stability**, **magnetism**, and **electronic gaps**. They pictorially describe (with red circles, conventionally) the full (aromatic) rings, versus the "empty" (non-aromatic) rings (without any coloring). The concept of AP is very old,[S2-S5] which has naturally evolved over the years.[22-25] To construct the APs (map of full and empty rings) we usually have first to decide on a local aromaticity descriptor and choose a "proper" threshold above (or below of) which the rings would be considered aromatic. A common or typical threshold for the absolute value |NICS(1)| could be 10 ppm (comparable to the values of benzene NICS(1) ~ -11 ppm) or 0.80 for HOMA (benzene value =1). In this scale, rings with $|NICS(1)| \geq$ 10 ppm are usually considered ("robust") aromatic, while rings with 6 ppm $\leq |NICS(1)| \geq$ 10 ppm are often described as "moderate aromatic". This could be highly debatable. To avoid such problems and other discrepancies, which are in fact irrelevant in the context of ERR, we use in this work a comparative reference point based on the $|NICS(1)|_{max}$ (or $|NICS(1)_{zz}|_{max}$) values for a given AGNR, instead of an absolute value based on the corresponding benzene numbers. Thus, for a particular AGNR, we select aromatic rings with NICS(1) values $|NICS(1)| \geq (0.75\text{-}0.80) \times |NICS(1)|_{max}$ in ppm, (or equivalently the same for $|NICS(1)_{zz}|$), whereas rings with |NICS(1)| or $|NICS(1)_{zz}|$ well above 50% of the corresponding maximum value we call them "half full" or "half empty" in order to avoid the term "moderate aromatic" which is usually connected with an implied range of NICS(1), as mentioned above. Thus, small values of |NICS(1)|, which are many

times problematic are considered as “empty”. The essential correctness of this choice is corroborated by the high success of ERR. Moreover, since we are targeting open shell states, we are using the corresponding open shell state APs of the AGNRs, and we group together nearby NICS(1) or $NICS(1)_{zz}$ for clarity and consistency. Thus, the clean and concise description of the diagram in Fig. 1 with “full” and “empty” rings is based in the raw results (i.e. NICS(1) and $NICS(1)_{zz}$) shown in Fig. S1.

As we can see in Fig. S1, APs are not sensitive to the exact choice of the aromaticity descriptor. Both NIC(1) and $NICS(1)_{zz}$ change in parallel producing the same APs It has been also illustrated[3] that both NICS(1) and $NICS(1)_{zz}$ are consistent with geometric[3] and energetic[9, 24] criteria of aromaticity as well. Moreover, any small differences (if any) are restricted to very-very small values[9], well below 50% of the threshold value, thus rendering APs practically independent of aromaticity-descriptor choice. Moreover, it is also important to observe that the choice of relative (not the absolute) threshold of aromaticity such $|NICS(1)|_{max}$ or $|NICS(1)_{zz}|_{max}$ is essential for ERR. For example, if we have used an absolute threshold based on benzene (-10 ppm) there would have been no working AP for the smallest AGNR (4x2). As a result, ERR could not be used efficiently, although we can recognize that ERR is fully working leading to two isoenergetic structures, one of which has already been synthesized.

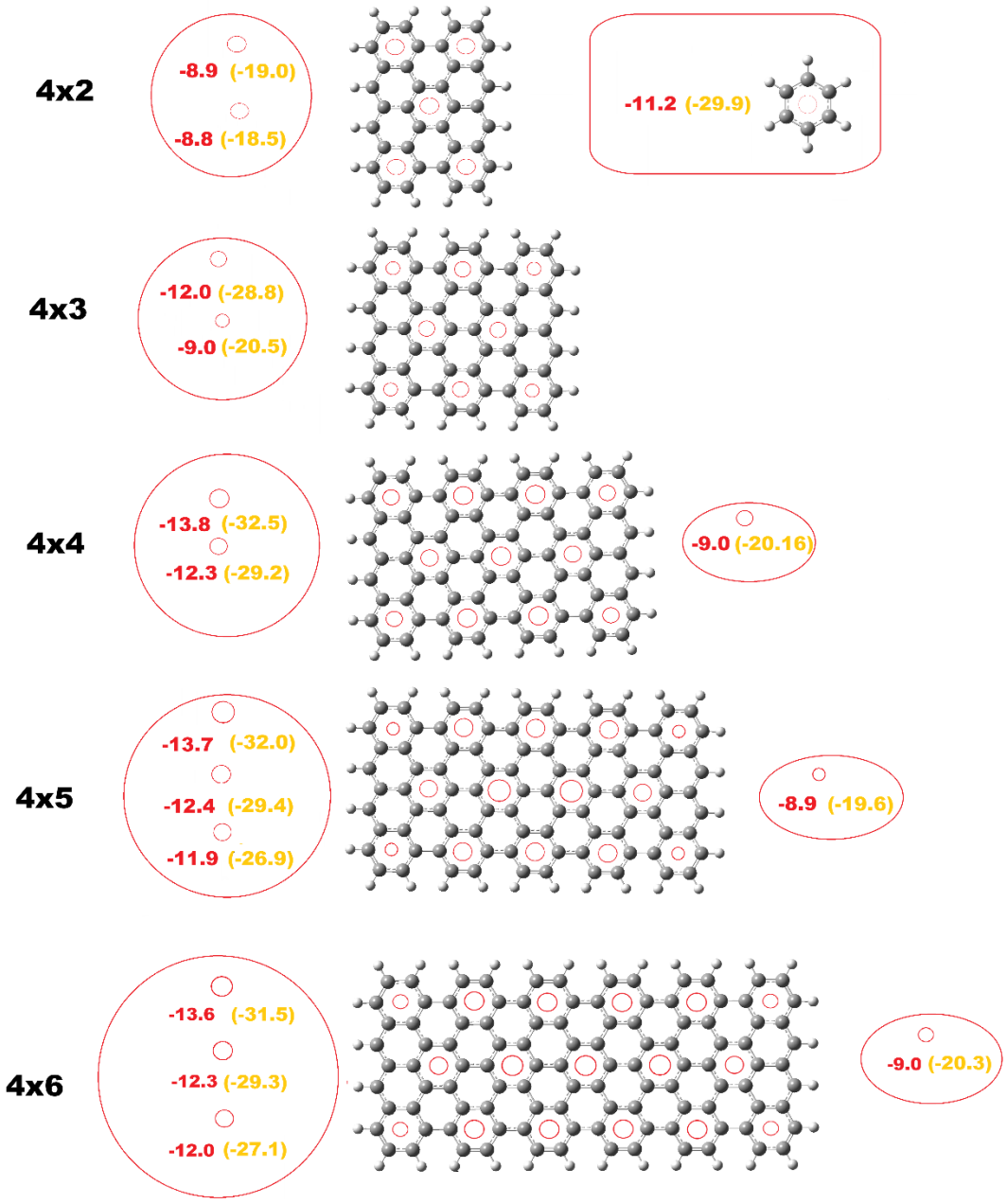

FIGURE S1. *Z=4 AGNRs for A=2-6. Aromaticity Patterns (APs) indicating NICS(1) and NICS(1)$_{zz}$ (in parenthesis) in ppm, showing ring grouping in aromatic (left) and "weakly" aromatic (right), which however in the present case is irrelevant for ERR, in contrast to the Z=3 case, discussed later. Benzene is also shown as a reference.*

§S2. Z=4 SW-AGNRs

§S2.1. The 4x2 SW-AGNRs

§S2.1.1 Structures of Lowest Energy and ERR.

Figure S2 shows the four lower-energy structures of the 4x2 SW-AGNRs and their relation to the corresponding 4x2 AGNR through ERR. Note that structures (a) and (b) which are respectively the current and previous[11, 8-9] lowest energy structures, fully obey ERR and are fully balanced electronically with zero dipole moments. The newly discovered (here) lowest energy structure (a), which is electronically balanced locally and globally, is slightly lower in energy than the previously established structure (b), has no zigzag bonds and is essentially a closed shell singlet. In contrast, structure (c), which only partly obeys ERR is not fully electronically balanced with an intrinsic dipole moment of 0.8 Debye. On the other hand, although structure (d) fully obeys ERR, it has an intrinsic dipole of -1.18 Debye and is even more distorted. This is apparently not related to aromaticity but to a locally and globally unbalanced charge distribution, due to local dipole-dipole repulsions. This is corroborated by the fact that in longer Z=4 SW-AGNRs with larger distance between local azulene dipoles, the corresponding structures have much lower total energy, almost isoenergetic with the lowest energy structure.

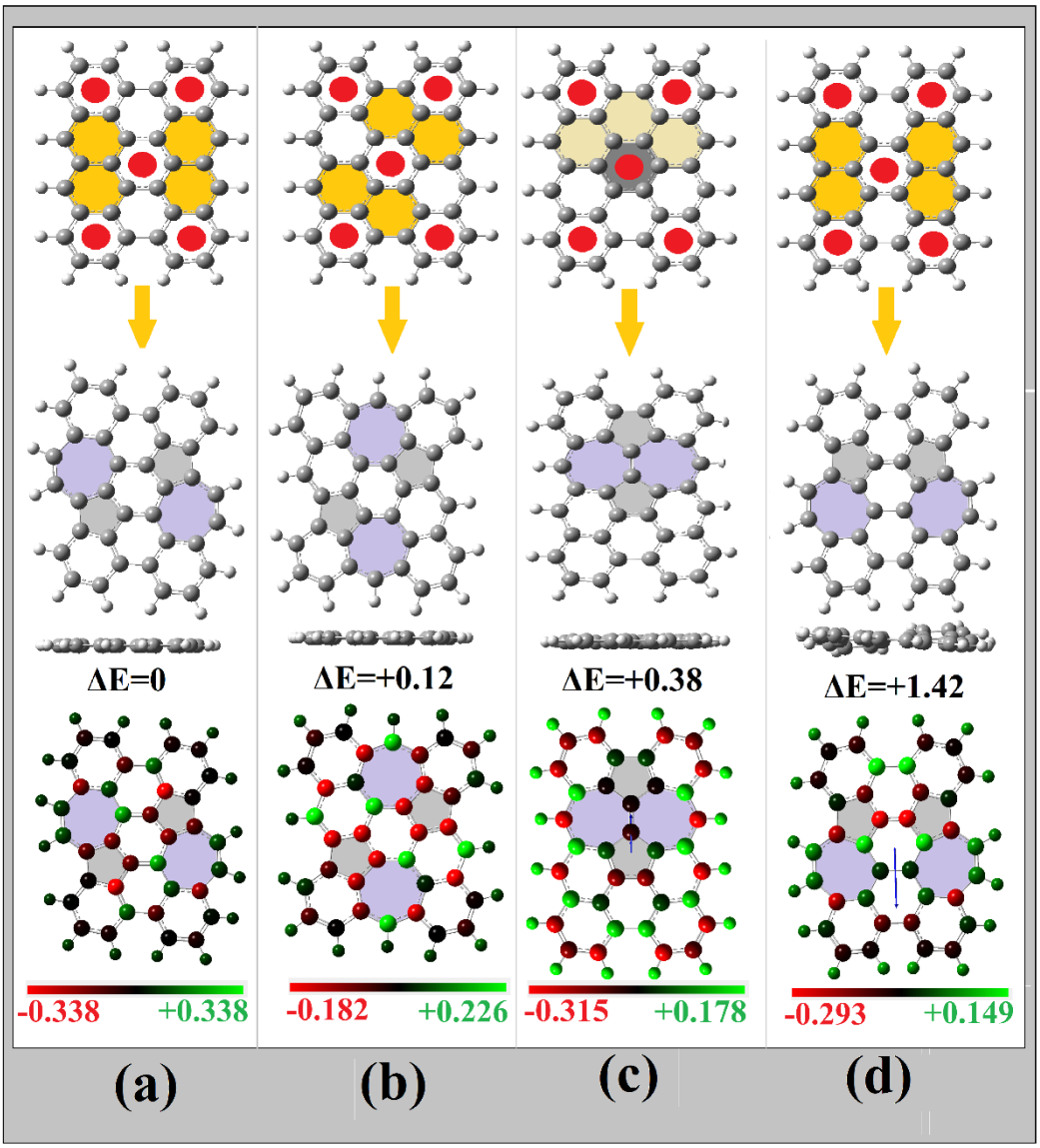

FIGURE S2. *Four low energy structures of 4x2 SW-AGNR generated by ERR from the benzenoid parent 4x2 AGNR (peri-tetracene) shown in the top part.*

The relevant empty rings of 4x2 AGNR for each SW-AGNR in the second row are emphasized by light yellow color, whereas the corresponding odd-membered non-alternant pentagonal and heptagonal rings are shaded grey and violet respectively. The structures in (a), (b), (c), and (d) are arranged in order of increasing energy shown below each structure. The Mulliken atomic charges for each structure are shown in the third row of the figure in a color range of red (for - charges) and green (for + charges), specified below each structure. The dipole moment, when is different than zero, as in structures (c) and (d), is indicated by a thin blue arrow.

Furthermore, with respect to structure (c), it is interesting to note that in other cases of SW-AGNRs with $Z \neq 4$, the same arrangement (with the compact azulene dimer) leads to very low or lowest energy structures because they are in these cases partly compatible with the ERR.

§S2.1.2. The Full Raman spectra of the lowest energy SW4x2 structures

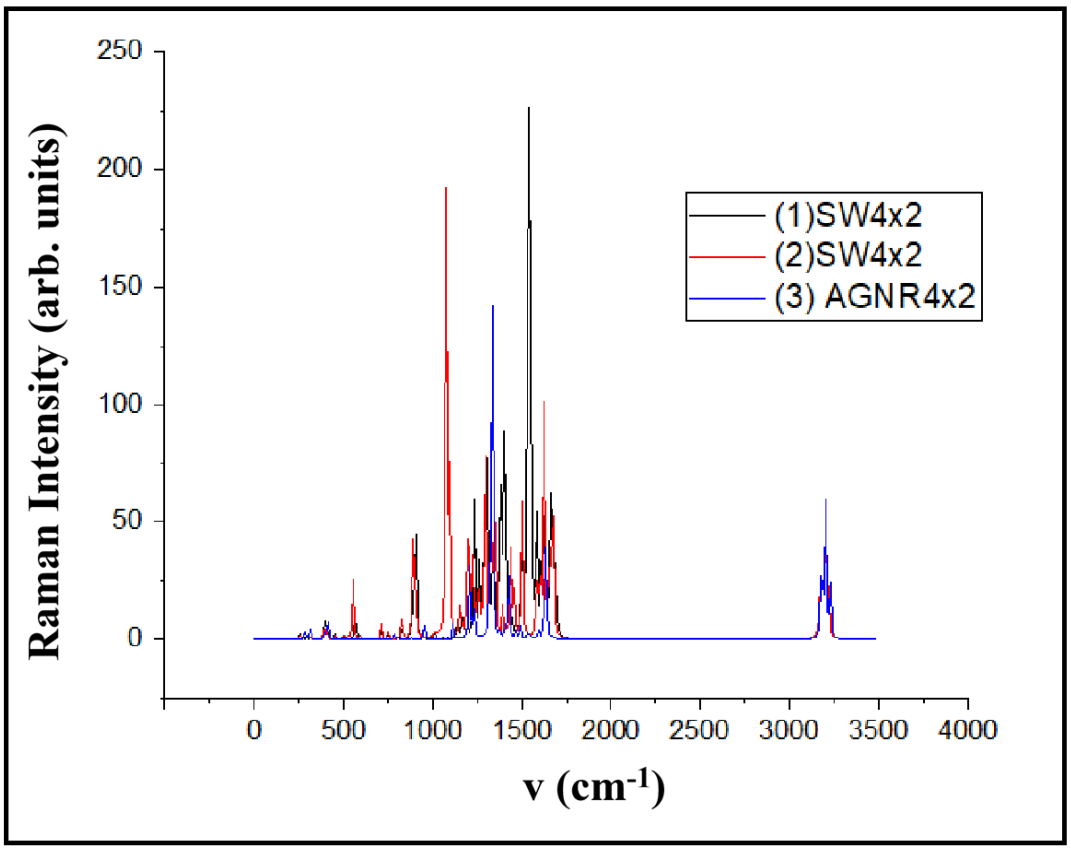

FIGURE S3. *Comparison of the Raman spectra in the range from 0 to 3500 cm^{-1} of the lowest energy 4x2 SW-AGNRs (1) in black color, and (2) in red color, together with the corresponding spectrum of the parent 4x2 AGNR (3) in blue color. The frequencies have not been scaled.*

§S3. Z=3 SW-AGNRs

§S3.1) The 3x2 SW-AGNRs

§S3.1.1. Structures of Lowest Energy.

Structure (1), which has been recently synthesized by Konishi *et al.*[12], is compatible (as much as possible) with ERR, in contrast to structures (2) and (3) which have been deliberately designed in complete disagreement to ERR (i.e. the azulene units have replaced full aromatic rings of the parent AGNR), and as a result they are much higher in energy (about 1.7 eV)

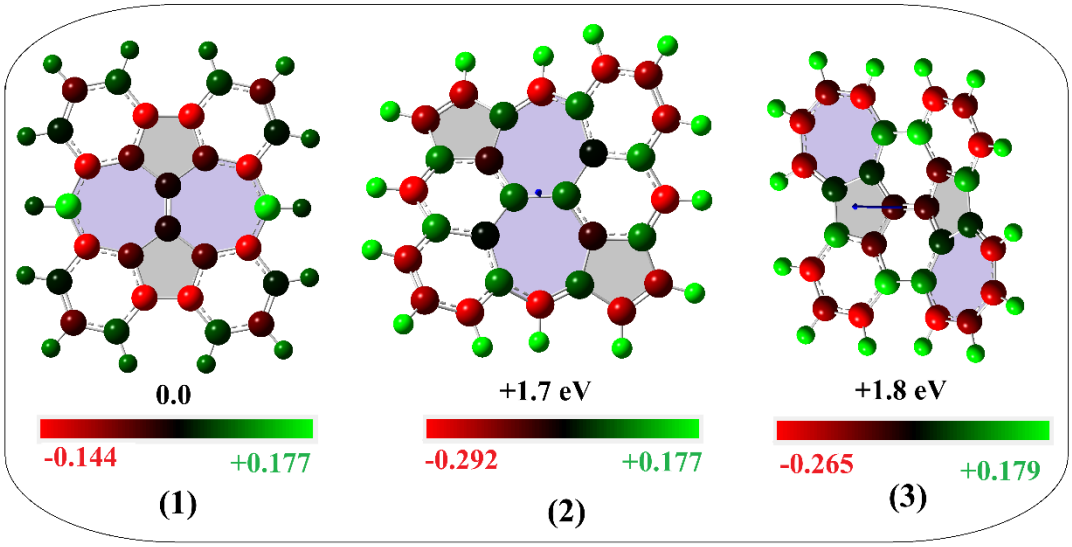

FIGURE S4. *Low energy structures of 3x2 SW-AGNR generated from the benzenoid parent 3x2 AGNR (Bisanthene), by ERR (1) and "anti-ERR" (2) and (3). The odd-membered pentagonal and heptagonal rings are shaded grey and violet respectively. The structures (1), (2) and (3) are arranged in order of increasing energy shown below each structure. The Mulliken atomic charges for each structure are shown in a color range of red (for - charges) and green (for + charges), specified below each structure. The dipole moment when is different than zero, in (2) and (3), is indicated by a thin blue arrow.*

§S3.1. Comparison of Raman Spectra

For purposes of possible characterization, the Raman spectra of the lowest energy 3x2 SW-AGNR are compared with the corresponding Raman spectra of the parent 3x2 AGNR, and the real lowest energy isomer (structure 2 in Fig. 1 or S1(b)) of 4x2 SW-AGNR:

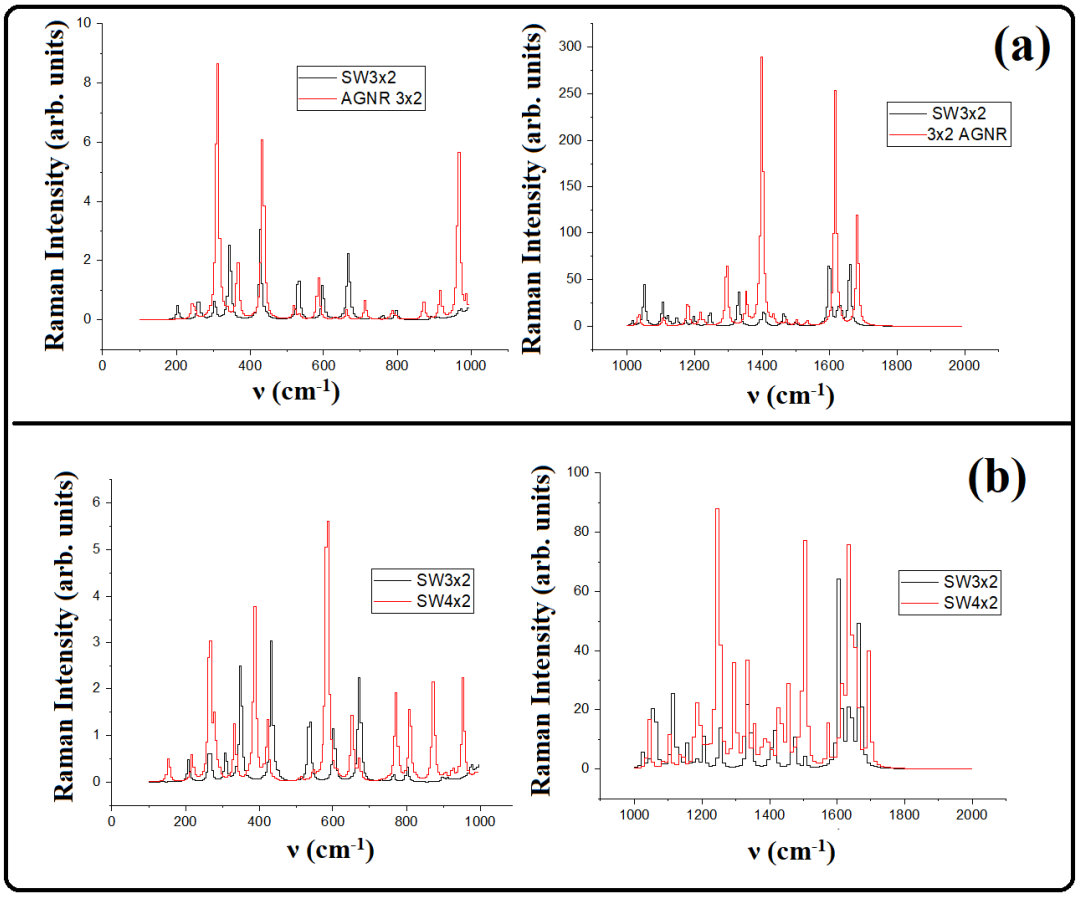

FIGURE S5. *Comparison of Raman spectra of 3x2 AGNR and SW- AGNRs in two frequency ranges for clarity (a), and 3x2 and 4x2 SW-AGNRs (b). Frequencies ν are given in* cm^{-1} *and Raman intensities in arbitrary units.*

S2.3. CO-type APs and the Concept of Partially Empty Rings.

- The Z=3 AGNRs are characterized by a with CO-type aromaticity pattern which can be considered as a superposition of (three) migrating sextets.[S5] They are characterized by more rings with significantly negative NICS(1) with a more continuous aromatic belt, in contrast to the more discrete nature of the CIRCO pattern in Z=4 AGNRs, where "full" NICS(1) are concentrated around $|NICS(1)|_{max}$ with stronger contrast. This is why the concept of partially empty rings becomes more important in this case, as is illustrated in Fig. S6

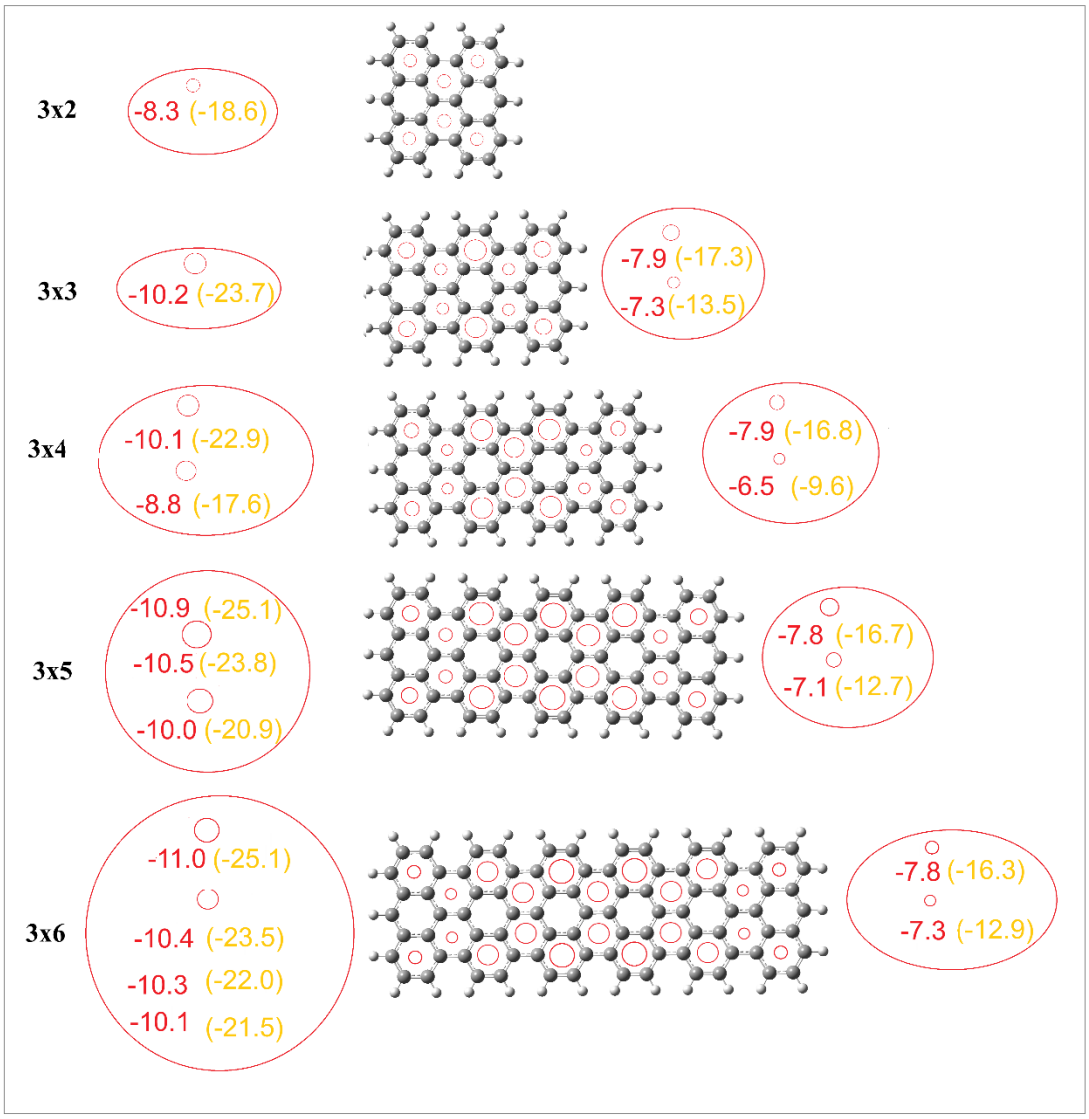

FIGURE S6. *Raw APs data for the Z=3 AGNRs, showing the grouping of the "Full" rings and "Partially empty" (or "partially filled") rings according to the raw NICS(1) and NICS(1)$_{zz}$ (in parenthesis) numbers in ppm.*

In Fig. S6 we can also verify that as length increases and more aromatic CO units keep added, the NICS(1) values keep increasing. This is a more general effect, and it happens also for the 4x SW-AGNRs as more CIRCO units are developed with increasing A. This could be interpreted as increasing aromaticity as the APs are getting enriched with more CO or CIRCO units. It could be concluded that increasing number of CO units in Coronene type APs, like CIRCO units in

Clar type APs, signifies "higher aromaticity" and the effect is not limited to only Clar-type APs. This increase should be also associated with higher stability. However, the values of binding energies in Tables 1 and 2 misleadingly show exactly the opposite effect which is dramatically reversed by the introduction of cohesive energies. So that increasing aromaticity ("measured" through $|\text{NICS}(1)|_{\max}$ or $|\text{NICS}(1)_{zz}|_{\max}$) is also associated with increased stability (expressed through ε_{coh}). It should be emphasized that the corner-rings values remain practically constant around -8.0 ppm independent of length. This is also true for the Z=4 AGNRs, where the NICS(1) values of the corner rings (with both armchair and zigzag bonds) are constant around -9.0 ppm, in that case. Yet, in all cases the NICS(1) numbers are always absolutely larger for Z=4 AGNRs compared to the corresponding values of the Z=3 AGNRs.

§S4. Cohesive Energy and Hydrogen(s) Chemical Potential

The cohesive energy ε_{coh} in Eq. (3) listed in Table 3 is defined through the total cohesive energy of Eq. (4) as:

$$E_{\text{coh}}[C_{N_C}H_{N_H}] = \text{B.E.}[C_{N_C}H_{N_H}] + \mu_H N_H. \qquad (4),$$

where $\text{B.E.}[C_{N_C}H_{N_H}]$ is the total binding energy given by Eq. (1), and μ_H is the chemical potential of hydrogen. The concept of cohesive energy is very old [S6-S9] associated with the "formation energy", especially of hydrogenated Si nanoparticles [S6, S8] and nanowires, [S7] as well as for carbon fullerenes. [S9] The chemical potential μ_H was originally specified either with respect to a reference structure (such as Silane SiH_4 or Methane CH_4 with corresponding μ_H values: 2.94 eV/atom and 4.53 eV/atom respectively), or was fitted to experimental data of formation energies. However, it was soon recognized that μ_H (like ε_{coh}) depends on size and bond topology. Therefore, for a given structure the preferred approach is to calculate the difference in total energies before and after the removal of the hydrogen atom under question.

Experience has shown that is better to remove a group of "similar" H atoms and divide afterwards by the number of H atoms removed. For Si nanowires μ_H varies from 2.90419 eV/atom to 3.55578 eV/atom, with an average value of μ_H =3.35 eV/atom,[S7] whereas for silicon fullerenes[S8] the average value is μ_H =3.46 eV/atom. For Carbon fullerenes[S9] with sp^3 bonding the average value is μ_H = 4.48 eV/ atom, compared to μ_H = 4.87eV/atom for benzene. For AGNRs (and SW-AGNRs) we have at least two groups of hydrogen for calculation μ_H, which obviously depends on the type of C–H bonding topology (e.g., armchair vs. zigzag). In such cases, Eq. (4) is generalized to Eqs. (S1, S2) by introducing distinct chemical potentials $\mu_{H_1}, \mu_{H_2}, \ldots$:

$$E_{coh}\left[C_{N_C}H_{N_H}\right] = B.E.\left[C_{N_C}H_{N_H}\right] + \mu_{H_1}.N_{H_1} + \mu_{H_2}\cdot N_{H_2} + \mu_{H_3}.N_{H_3} + \ldots \quad \text{(S1)}\,,$$

with: $N_{H_1} + N_{H_2} + N_{H_3} + \cdots = N_H$ (S2) .

For hexagonal PAHs the values of the chemical potentials $\mu_{H_1} \equiv \mu_{H_{armchair}}$ varies between -4.98 eV/atom and -5.38 eV/atom, whereas $\mu_{H_2} \equiv \mu_{H_{zigzag}}$ remains practically constant around the value $\mu_{H_{zigzag}}$ =-6.3 eV/atom.

For AGNRs $\mu_{H_{armchair}}$ varies between 4.94 and 5.09 eV/H-atom and $\mu_{H_{zigzag}}$ between 5.22 eV/H-atom and 5.83 eV /H-atom, shown in Table S1 below. As you can see in Table S1 there are no significant differences with width (Z) variation for a given length A, but always $|\mu_{H_{zigzag}}| > |\mu_{H_{armchair}}|$.

Table S1. *H-Chemical potentials* $\mu_{H_{armchair}}$ *and* $\mu_{H_{zigzag}}$ *and for AGNRs*

PBE0 / 6-311g(d, 2p)	$\mu_{H_{armchair}}$ **(eV/atom)**	$\mu_{H_{zigzag}}$ **eV/atom)**
3x2-AGNR	-5.05	-5.41

3x4 - AGNR	-4.97	-5.83
3x6 - AGNR	-4.94	-5.32
═══	═══	═══
4x2 - AGNR	-5.09	-5.22
4x4 - AGNR	-4.97	-5.78
4x6 - AGNR	-4.96	-5.30

§S5. Examples of Cohesive Energy and Hydrogen-Chemical-Potential-Calculations.

§S5.1 The 4x4 AGNR

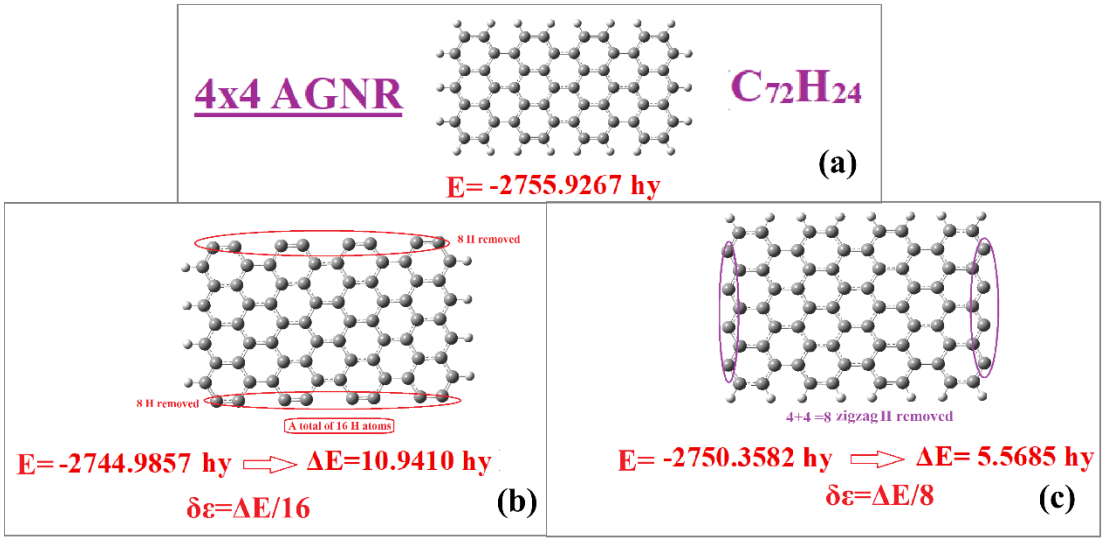

FIGURE S7. *Simple comprehensive diagram for the calculation of* $\mu_{H_{armchair}}$, $\mu_{H_{zigzag}}$ *and cohesive energy* ε_{coh} *for the 4x4 AGNR (a), by removing armchair (b) and zigzag (2) Hydrogens. Total energies E, energy differences ΔE, and energy differences per hydrogen atom δε, are given in hy (a.u.), calculated at the PBE0/6-311g(d,2p) level, shown below each structure.*

§5.1.1 $\mu_{H_{armchair}}$ $\mu_{H_{zigzag}}$ and calculations

Besides the energies in the diagram of Fig. S7, we also need the carbon and hydrogen atoms total energies:

C- atom energy at the level of PBE0/6-311g(d,2p) = E_C = -37.801871 Hy

and H- atom energy at the level of PBE0/6-311g(d,2p) = E_H = -0.501038 Hy

Total Energy = -2755.9267 hy → E_b ($C_{72}H_{24}$) =22.167076 hy →

$\varepsilon_b(C_{72}H_{24})$/C-atom=-0.30780555 hy/atom= 8.3742287111 eV/atom

§5.1.2 $\mu_{H_{armchair}}$ $\mu_{H_{zigzag}}$ and calculations

From Fig. S7.b we have: δε=-0.6838125 → $\mu_{H_{armchair}}$ = -0.182774 hy/H-atom=-4.97 eV/ H-atom. Similarly, from Fig. S7.c we find:

δε= -0.6960625 hy/H-atom → $\mu_{H_{zigzag}}$ = -0.1950245 hy/atom = -5.3046664 eV/H-atom.

§5.1.3 ε_{coh} calculation

From eq. S1 and the binding energy E_b ($C_{72}H_{24}$), found above, we get:

$\varepsilon_{coh}(C_{72}H_{24})$ =0.24559011 hy /C-atom = 6.68005102 eV /C-atom

§S5.2 The 4x4 SW-AGNR

For SW-AGNRs on top of armchair and zigzag hydrogens we have also to distinguish between "normal" hydrogens and hydrogens on non-hexagonal rings. In Fig S8 this procedure is illustrated schematically.

Comparing the total energies in Figs. S8 (a) and S8(b) we find:

ΔE= 2.704797 hy → δε=ΔE/4= -0.67619 hy. Thus, μ_{H4} = 0.17516125 hy/H-atom=4.76438 eV/H-atom. Similarly comparing the energies in Figs. S8 (a) and S8 (c) we find: ΔE= 8.275646 hy → δε=ΔE/12 = -0.689637. Therefore, μ_{H12} = -0.18859916 hy/H-atom =-5.12989 eV/H-atom.

Finaly, from Fig. S8 (d) we find: ΔE= 5.447519 hy → δE=-0.68093987 and μ_{H8} = -0.179902 hy/H-atom, or μ_{H8} = -4.8933 eV/H-atom.

Therefore: ε_{coh} (sw$C_{72}H_{24}$)= 6.6697520 eV/atom.

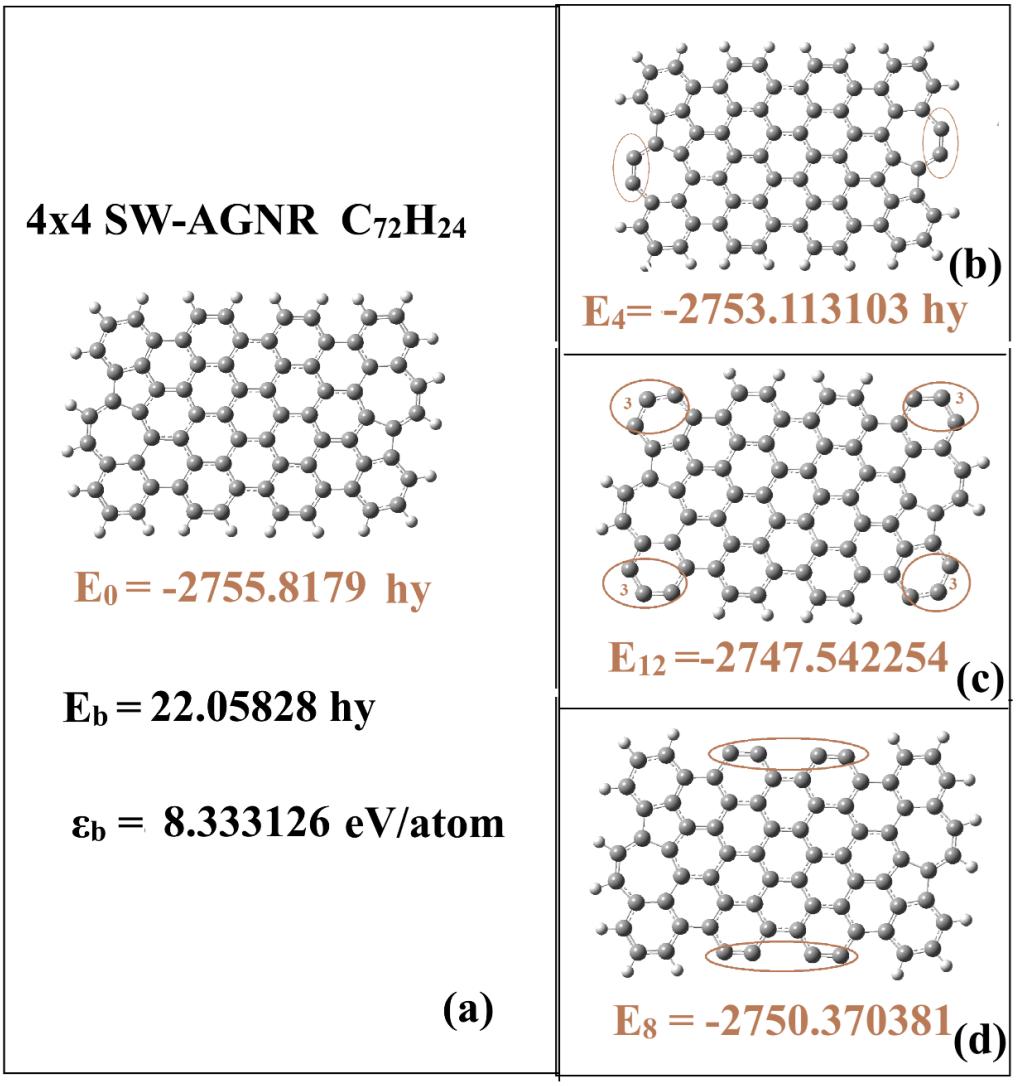

FIGURE S8. *Simple schematic diagram for the calculation of* $\mu_{H_{heptagon}}$, $\mu_{H_{corner}}$, $\mu_{H_{armchair}}$, *and cohesive energy* ε_{coh} *for the 4x4 SW-AGNR (a), by removing heptagonal (b), corner (c) and armchair (d) Hydrogens, in full analogy to Fig. S7. Total energies E, energy differences ΔE, and energy differences per hydrogen atom δε, are given in hy (a.u.), calculated at the PBE0/6-311g(d,2p) level, shown below each structure.*

§S5.3 Aromaticity and Stability

It has been illustrated earlier by the present author[24] that if we use NICS(1) (or $NICS(1)_{zz}$ as a local aromaticity descriptor we can then make an overall aromaticity assessment by considering

the extreme or the average NICS(1) number ($|NICS(1)|_{max}$ and $<|NICS(1)|>$ respectively) as an overall ("global") aromaticity measure which has the advantage to be fully compatible with the overall measure of stability through ε_{coh} , which is rather unusual. In other words, if we adopt $|NICS(1)|_{max}$ as a "global" aromaticity assessment of a given PAH or NGR, and ε_{coh} as a valid index of stability, then aromaticity and stability vary in unison, following the same trends (in contrast to total energy or binding energy). This is corroborated by the results in Table 3 and Fig. 4 and Fig. S9 below.

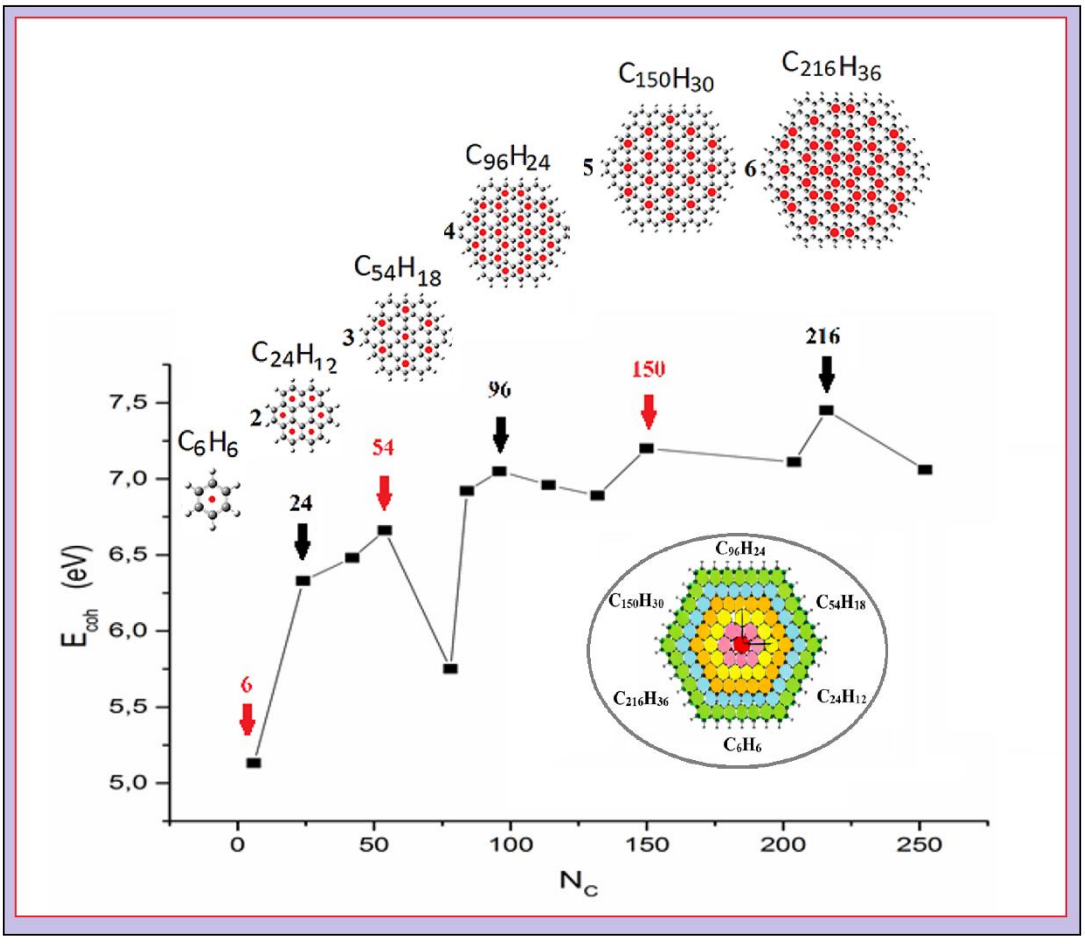

FIGURE S9. *Full size version of the Variation of cohesive energy, eq. (5), in eV, in terms of N_C (the number of carbon atoms=number of π-electrons) of Fig. 4, enriched with the structures and APs of the "magic PAHs" and the Shell structure. Maxima correspond to "shell closure" occurring for "magic" PAHs.[24] Similarly to Fig. 4, the maxima at "magic" PAHs are indicated by vertical arrows.*

We should recall that shells 2 and 3 (coronene, and circocoronene) correspond to AGNRs with Z=3 and 4, respectively (see ref. 19) and the corresponding AGNRs and SW-AGNRs in Table 3 follow exactly the same trends (i.e. higher cohesive energy and -NICS(1)$_{max}$ for the CIRCO APs). Likewise recall that the peaks in Fig. 4 and Fig. S9 correspond to shell change (increase), in contrast to Z=3 AGNRs (and similarly to Z=4 AGNRs) which remain within the same shell (the same Z). As a result, |NICS(1)|$_{max}$ and ε_{coh} , increase regularly and smoothly (without peaks) in this case.

§S6. 2x AGNRs and SW-AGNRs

§S6.1 Energetic Characteristics

The full energies and energy differences of the structures in Fig.5 are given in Table S2 below:

TABLE S2. *Total energies* E_{tot}*(a.u.), relative energies* ΔE_{tot}*(eV), binding energies* ε_b*(eV/atom), and binding-energy differences* $\delta\varepsilon_b$*(eV/atom) for the lowest-energy Z = 2 SW-AGNRs (A = 2–6), compared to the corresponding parent AGNRs. All structures optimized at the PBE0/6-311G(d,2p) level.*

A = 2 (2×2, $C_{20}H_{12}$)

Structure	E_{tot} (a.u.)	ΔE_{tot} (eV)	ε_b (eV/atom)	$\delta\varepsilon_b$ (eV/atom)
Parent AGNR	-768.66342	0	8.994	0
SW-2×2 (1)	-768.56898	2.6	8.865	0.128
SW-2×2 (2)	-768.54795	3.1	8.837	0.157

A = 3 (2×3, $C_{30}H_{16}$)

Structure	E_{tot} (a.u.)	ΔE_{tot} (eV)	ε_b (eV/atom)	$\delta\varepsilon_b$ (eV/atom)
Parent AGNR	-1151.8138	0	8.832	0
SW-2×3 (1)	-1151.6895	+3.4	8.719	0.113
SW-2×3 (2)	-1151.6699	+3.9	8.701	0.131

A = 4 (2×4, $C_{40}H_{20}$)

Structure	E_{tot} (a.u.)	ΔE_{tot} (eV)	ε_b (eV/atom)	$\delta\varepsilon_b$ (eV/atom)
Parent AGNR	-1534.9650	0	8.751	0
SW-2×4 (1)	-1534.8627	+2.8	8.682	0.070
SW-2×4 (2)	-1534.8577	+2.9	8.678	0.073

A = 5 (2×5, $C_{50}H_{24}$)

Structure	E_{tot} (a.u.)	ΔE_{tot} (eV)	ε_b (eV/atom)	$\delta\varepsilon_b$ (eV/atom)
Parent AGNR	-1918.1165	0	8.703	0
SW-2×5 (1)	-1917.9942	+3.4	8.636	0.068
SW-2×5 (2)	-1917.9921	+3.5	8.635	0.070

A = 6 (2×6, $C_{60}H_{28}$)

Structure	E_{tot}(a.u.)	ΔE_{tot} (eV)	ε_b (eV/atom)	$\delta\varepsilon_b$ (eV/atom)
Parent AGNR	-2301.2682	0	8.671	0
SW-2×6 (1)	-2301.1668	+2.8	8.625	0.046
SW-2×6 (2)	-2301.1607	+2.9	8.622	0.049

Comparing the binding energy differences between SW-AGNRs and the corresponding AGNRs we can immediately deduce that Z=2 SW-AGNRs should be much more difficult to synthesize from their parent AGNRs, compared to Z=3 and (much more) Z=4 ones, especially the very short ones for which $\delta\varepsilon_b$ is at least one order of magnitude larger.

§S6.2 Aromatic Characteristics: Empty and "partially empty" Rings of the parent Z=2 AGNRs.

The detailed NICS(1) and NICS(1)$_{zz}$ values of Z=2 AGNRs are shown in Fig. S10. We observe that the $|NICS(1)|_{max}$ values at the center of the even-A AGNRs, keep increasing with increasing A. In contrast, the $|NICS(1)|_{max}$ values at the ends of the odd-A AGNRs remain constant, at a clearly lower value (9.6 ppm). This seems to be true also for their central "partially empty" rings.

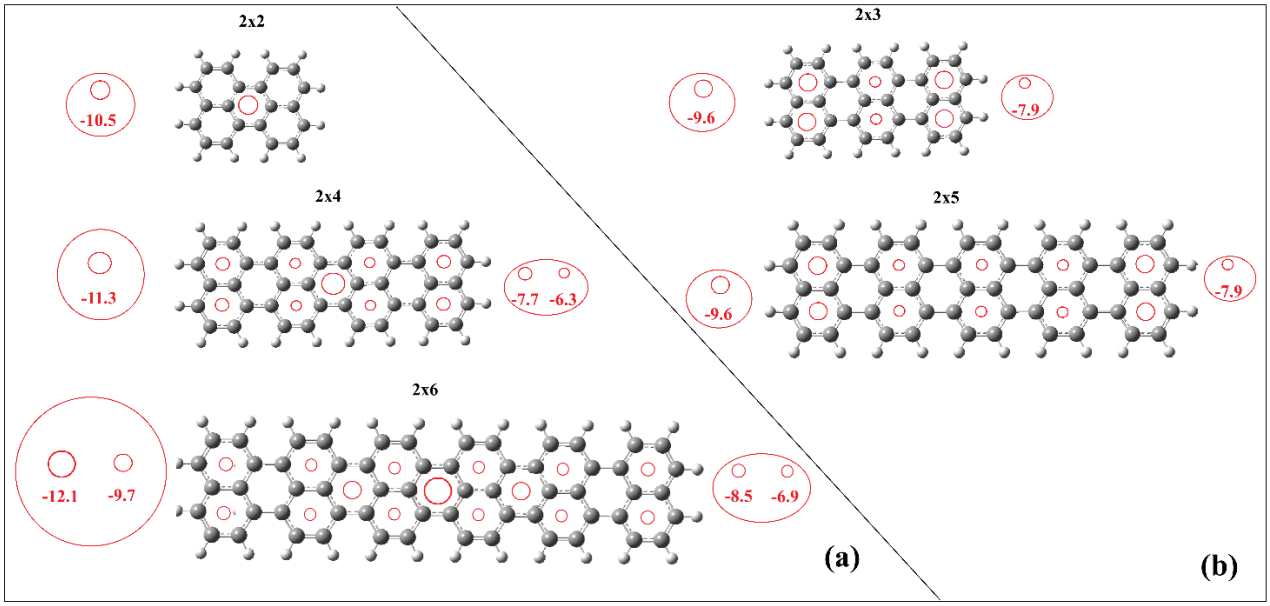

FIGURE S10. *Raw APs data, showing the grouping of the "Full" rings and "Partially empty" (or "partially filled") rings according to the raw NICS(1) numbers in ppm of even-A (a) and odd-A (b) 2x AGNRs.*

SI REFERENCES

S1. Gaussian 16, Revision C.01, Frisch, M. J.; Trucks, G. W.; Schlegel, H. B.; Scuseria, G. E.; Robb, M. A.; Cheeseman, J. R.; Scalmani, G.; Barone, V.; Petersson, G. A.; Nakatsuji, H.; Li, X.; Caricato, M.; Marenich, A. V.; Bloino, J.; Janesko, B. G.; Gomperts, R.; Mennucci, B.; Hratchian, H. P.; Ortiz, J. V.; Izmaylov, A. F.; Sonnenberg, J. L.; Williams-Young, D.; Ding, F.; Lipparini, F.; Egidi, F.; Goings, J.; Peng, B.; Petrone, A.; Henderson, T.; Ranasinghe, D.; Zakrzewski, V. G.; Gao, J.; Rega, N.; Zheng, G.; Liang, W.; Hada, M.; Ehara, M.; Toyota, K.; Fukuda, R.; Hasegawa, J.; Ishida, M.; Nakajima, T.; Honda, Y.; Kitao, O.; Nakai, H.; Vreven, T.; Throssell, K.; Montgomery, J. A., Jr.; Peralta, J. E.; Ogliaro, F.; Bearpark, M. J.; Heyd, J. J.; Brothers, E. N.; Kudin, K. N.; Staroverov, V. N.; Keith, T. A.; Kobayashi, R.; Normand, J.; Raghavachari, K.; Rendell, A. P.; Burant, J. C.; Iyengar, S. S.; Tomasi, J.; Cossi, M.; Millam, J. M.; Klene, M.; Adamo, C.; Cammi, R.; Ochterski, J. W.; Martin, R. L.; Morokuma, K.; Farkas, O.; Foresman, J. B.; Fox, D. J. Gaussian, Inc., Wallingford CT, **2016.**

S2. Watson, M. D.; Fechtenkoetter, A.; and Mullen, K. Big Is Beautiful-Aromaticity Revisited from the Viewpoint of Macromolecular and Supramolecular Benzene Chemistry. Chem. Rev. 2001, 101, 1267−130

S3. Balaban, A.T., CLAR FORMULAS: HOW TO DRAW AND HOW NOT TO DRAW FORMULAS OF POLYCYCLIC AROMATIC HYDROCARBONS. *Polycyclic Aromatic Compounds,* **2004**, 24: 83–89, 2004 DOI: 10.1080/10406630490424124

S4. Stein, S. E. and Brown R. L. π-Electron Properties of Large Condensed Polyaromatic Hydrocarbons, J. Am. Chem. Soc. **1987**, 109, 3721-3729

S5. Moran, D. ; Stahl, F. ; Bettinger, H. F.; | Henry F. Schaefer III, H. F.; and Schleyer, P. v. R. Towards Graphite: Magnetic Properties of Large Polybenzenoid Hydrocarbons. J. Am. Chem. Soc. **2003**, 125, 6746-6752

S6. Puzder, A. J. Williamson, F. A. Reboredo, and G. Galli, *Phys. Rev. Lett.* **2003**, 91, 157405 2003.

S7. Zdetsis A. D. High-symmetry low-energy structures of C60H60 and related fullerenes and nanotubes, Phys. Rev. B 2008, 77, 115402 1-5. DOI: 10.1103/PhysRevB.77.115402

S8. Zdetsis, A. D. , Koukaras E. N., Garoufalis, C. S. Structural properties and magic structures in hydrogenated finite and infinite silicon nanowires, Appl. Phys. Lett. 2007, 91, 203112. DOI: 10.1063/1.2813019

S9. Zdetsis, A. D. One-nanometer luminous silicon nanoparticles: Possibility of a fullerene interpretation, Phys. Rev. B 2009 79, 195437. DOI: 10.1103/PhysRevB.79.19543